Identifying the Origin of Iris Images Based on Fusion of Local Image Descriptors and PRNU Based Techniques

Christof Kauba, Luca Debiasi and Andreas Uhl
Department of Computer Sciences
University of Salzburg, Austria
{ckauba, ldebiasi, uhl}@cosy.sbg.ac.at

Abstract

Being aware of the origin (source sensor) of an iris images offers several advantages. Identifying the specific sensor unit supports ensuring the integrity and authenticity of iris images and thus detecting insertion attacks at a biometric system. Moreover, by knowing the sensor model selective processing, such as image enhancements, becomes feasible. In order to determine the origin (i.e. dataset) of near-infrared (NIR) and visible spectrum iris/ocular images, we evaluate the performance of three different approaches, a photo response non-uniformity (PRNU) based and an image texture feature based one, and the fusion of both. Our first set of experiments includes 19 different datasets comprising different sensors and image resolutions. The second set includes 6 different camera models with 5 instances each. We evaluate the applicability of the three approaches in these test scenarios from a forensic and non-forensic perspective.

1. Introduction

A typical biometric system consists of three main components: a biometric sensor to capture the raw biometric data, a feature extractor that converts the raw data to a feature based representation and a matcher which compares 2 sets of features and outputs a score value corresponding to the similarity or dissimilarity of the the feature sets. We focus on the first component, the biometric sensor itself, specifically in iris recognition. The base component of iris sensors deployed in practical applications is a digital image sensor to acquire the iris images, commonly supported by a near infra-red (NIR) light source to improve the iris recognition results [8].

Digital image forensics deals with still images and analysing traces in still image data. These traces are extracted merely from structural analysis of image files and statistical analysis of the image data (i. e. pixel values). Deducing sensor information from the iris images serves as a basis for different forensic and non-forensic tasks. One of the major tasks in digital image forensics is establishing an image's origin with the help of the deduced sensor information. This can be performed at different levels: Sensor technology, brand, model, unit. In the context of biometric systems the extracted sensor information can be used for various applications. In this work we focus on two specific ones: Securing an iris recognition system against insertion attacks and enabling device selective processing of the image data.

The authenticity and integrity of the acquired iris images plays an important role for the overall security of a biometric system. Ratha *et al*. [31] identified eight stages in a generic biometric system where attacks may occur. An insertion attack bypasses the biometric sensor by inserting data (biometric sample) into the transmission from the sensor to the feature extractor. This transmission is the most relevant point for an attack on the integrity and authenticity of the acquired iris images, where the iris image inserted during the attack could be acquired with another sensor off-site, even without the knowledge of a genuine user, or be a manipulated image to spoof the biometric recognition system.

In large-scale biometric system various sensors from different manufacturers and models are deployed and the interoperability is often affected by specifics of each sensor, such as the acquisition technique or in-sensor image processing. Selective processing of the iris images helps to improve the interoperability by applying a sensor tailored biometric tool chain. Therefore information about the sensor model is required, which can be deduced from the iris images directly utilising image forensic methods.

This work evaluates the feasibility of deducing sensor information at model and unit level, i.e. the sensor an image is captured with, from the iris/ocular image using PRNU and image texture based methods. Our approach differs from existing literature in the following ways: (a) we consider both, a PRNU and an image texture based (IT) approach and analyse their strengths and weaknesses; (b) we include a larger number of iris datasets/sensors (19 datasets) and additional image forensic benchmark dataset; (c) we evaluate a fusion of the PRNU and the IT based approach to overcome the weaknesses of each single approach; (d) we consider different training set sizes down to 1 training image and different patch sizes for extracting the PRNU and the image texture features are compared; (e) we discuss the applicability of each approach as a mean of insertion attack prevention and in the context of selective processing.

The rest of the paper is organised as follows: Related work is summarised in Section 2. Section 3 describes the two different classification approaches. The experimental setup including the examined iris data sets is listed in Section 4. The results are illustrated and an application specific discussion is given in Section 5. Finally Section 6 concludes this paper.

2. Related Work

To determine an image's origin on unit level several approaches have been proposed exploiting hardware and software related artifacts. The PRNU is an intrinsic property of all digital imaging sensors due to slight variations among individual pixels in their sensitivity to incoming illumination. Consequently, every sensor casts a unique, weak, noise-like pattern onto every image it takes. This pattern, which can be regarded as a "sensor fingerprint", is essentially an unintentional stochastic spread-spectrum watermark that survives processing, such as lossy compression, filtering or white-balancing. A sensor's fingerprint can be estimated from several images taken by the sensor and later detected in a given image to establish image origin and integrity.

Novel sensor identification approaches are based on Deep Convolutional Neural Networks (CNN). Tuama *et al.* [33] proposed to extract the noise residuals with a high-pass filter and classify the images using a CNN. However, this approach relies on a large number of images for the CNN training step, which limits the application scenarios for these approaches.

In the context of biometric systems security, the PRNU fingerprint of a sensor can be utilised to ensure the integrity and authenticity of images acquired with a biometric sensor. Höller *et al.* [34] propose a suitable passive approach to secure the transmission channel between the sensor and the feature extractor, making use of sensor fingerprints based on a sensor's PRNU [4].

To ensure the authenticity of the biometric sensor, first the discriminative power of the biometric sensors has to be evaluated, as it has been done in [3] and [34] using the PRNU. The results from Höller *et al.* [34], where the discriminative power of five iris sensors from the *CASIA-Iris V4* database [25] has been evaluated, show high variations. Other work by Kalka *et al.* [16] regarding the differentiability of iris sensor showed varying results. Some possible explanations are given in [16] and [34] and include highly correlated data of biometric datasets, saturated pixels and the use of multiple sensors of the same model. An additional caveat for the PRNU extraction is the image content. Since the PRNU covers the high frequency components of an image, it is contaminated with other high frequency components within the images, such as edges.

Banerjee and Ross [2] evaluated multiple PRNU estimation schemes for identifying sensors from iris images. They used 12 different datasets, 4 PRNU extraction methods and investigated dataset specific artefacts as well as the effect of a photometric transformation. They were able to identify the sensor for a majority of the datasets.

In the context of selective image processing, where it is sufficient to determine the sensor model (i.e. iris dataset), El-Naggar and Ross [11] proposed a passive approach tailored to iris recognition. At first the ocular image is segmented to get the iris region, then the iris texture is unwrapped, followed by a normalisation step to get a normalised iris image. Out of the inner half of this normalised iris image a feature vector containing statistical and Gabor features is extracted and then classified using a 3-layer artificial neural network. They were able to achieve accuracies of $80 - 85\%$.

Marra *et al.* [22] propose a CNN-based technique including transfer learning to identify the iris sensor model from iris images. They map the features extracted from images captured by one sensor to images captured by a different one. They investigated 9 different sensor models. They achieve promising results, enabling a model-adaptive preprocessing of the iris images to obtain seamless sensor interoperability.

To overcome problems in cross-sensor matching in large-scale iris recognition systems Arora *et al.* [1] developed an iris camera classification-based preprocessing framework. Using the output of their statistical image-feature based camera classification they apply a device-specific iris image enhancement leading to a significant improvement in recognition accuracy.

3. Classification Techniques

In this section we present two different techniques each allowing to infer which dataset an iris image originates from. The first technique, called PRNU based Sensor Identification (PSI), achieves this by utilising non unique artefacts embedded in the images. The second technique, Image Texture Classification (ITC), makes use of image texture information and its inherent features. Both techniques are presented in detail in the following.

3.1. PRNU based Sensor Identification (PSI)

A digital image sensor consists of lots of small photosensitive detectors, commonly known as pixels. Due to imperfections in the manufacturing and the inhomogeneity of the manufacturing material, silicon, the efficiency of each pixel in converting photons to electrons varies slightly. This slight variation is commonly known as photo-response non-uniformity (PRNU). The extraction of the PRNU noise residuals is performed as indicated by Fridrich in [13]. For each image I the noise residual W_I is estimated:

$$W_I = I - F(I) \tag{1}$$

where F is a denoising function filtering out the sensor pattern noise. Different denoising filters have been used for the extraction of the PRNU noise residual [7, 13, 24].

The extracted PRNU noise residual is then normalised in respect to the L_2-norm because its embedding strength is varying between different sensors as explained by [34].

The PRNU fingerprint $\hat{K}$ of a sensor, which isolates the systematic components and suppresses random noise, is then estimated using a maximum likelihood estimator for images I_i with $i = 1...N$.

$$\hat{K} = \frac{\sum_{i=1}^{N} W_{I_i} I_i}{\sum_{i=1}^{N} (I_i)^2} \tag{2}$$

To determine if an image has been acquired with a specific sensor, the presence of a sensor's PRNU fingerprint in the questioned image has to be detected. Since images acquired with iris sensors are usually not geometrically transformed, this can be done by means of calculating the normalised Cross Correlation (NCC) between between a PRNU noise residual of an Image J and a PRNU fingerprint weighted by the image content of J.

Furthermore, different PRNU enhancement techniques have been applied to the noise residuals and PRNU fingerprints in order to suppress undesired artifacts [19, 20].

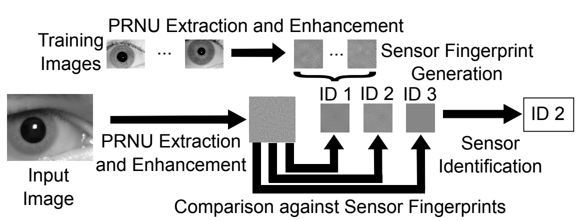

Figure 1. PRNU noise residual extraction and identification of corresponding sensor.

3.2. Image Texture Classification (ITC)

The ITC approach is SVM based, thus a training phase is needed, similar to generating a PRNU fingerprint for the PSI approach. The input are the iris/ocular images and the output is a prediction of the iris sensor used to capture the image or the dataset where the input iris image belongs to, respectively. In the following the three feature extraction methods, namely DenseSIFT, DMD and LBP are briefly explained. Then the classification approach using a GMM, Fisher Vector encoding and an SVM classifier is described.

3.2.1 Feature Extraction

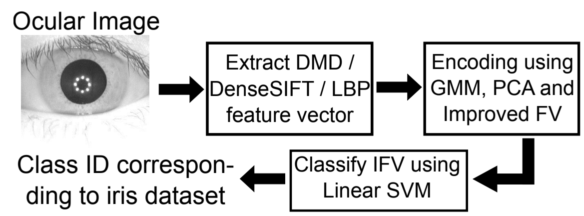

Figure 2. Flowchart of the Image Texture Classification (ITC) approach.

DSIFT: Fei-Fei et al. [12] proposed to use the local SIFT descriptors, a general purpose feature extraction technique used in object recognition [21], at multiple scales on a predefined grid defined across the whole image instead of localising their positions according to scale space extrema.

DMD: Dense Micro-block Difference is a local feature extraction and texture classification technique proposed by Mehta and Egiazarian [23] to capture the repetitively characteristic local structure providing discriminative information.

LBP: The local binary patterns proposed by Ojala [27] observe the variations of pixels in a local neighbourhood. These variations are thresholded against the central pixel value to obtain a binary decision, which is then encoded as a scalar value. The occurrences of each scalar value for all pixels in the image are represented in a histogram, which forms the extracted feature vector.

3.2.2 Feature Encoding

We utilise the Improved Fisher Vector Encoding (IFV) scheme in the same way as in [5]. At first the respective features (DSIFT, DMD, LBP) are extracted to obtain a feature vector f. For standard Fisher Vector (FV) encoding the feature vector f is soft-quantised using a Gaussian Mixture Model (GMM) with K modes where the Gaussian covariance matrices are assumed to be diagonal. The local descriptors present in f are first decorrelated and then dimensionality reduced (optional) by PCA. The IFV now adds signed square rooting and l^2 normalisation. For more details the interested reader is referred to [5].

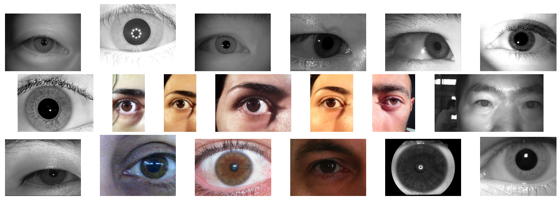

Figure 3. Sample images from different datasets.

Dataset Name	#IMG	Sensor	ILM	Resolution	CID
CASIA V2 [25]	1200	OKI IRISPASS-h	NIR	480x640	1
CASIA V3 [25]	2639	CASIA Iris camera	NIR	320x280	2
CASIA V4 [25]	20000	IrisKing IKEMB-100	NIR	640x480	3
CSIR 1 [26]	4000	EyeGuard AD100	NIR	640x480	4
CSIR 2 [26]	4000	IKEMB220	NIR	640x480	5
ICE [28]	2953	LG EOU 2200	NIR	480x640	6
IITD [18]	1120	JIRIS, JPC1000	NIR	240x320	7
MICHE S1 [9]	626	Samsung Galaxy S4 F	VL	various	8
MICHE S2 [9]	628	Samsung Galaxy S4 R	VL	various	9
MICHE S3 [9]	632	Samsung Galaxy Tab2	VL	various	10
MICHE I1 [9]	619	Apple iPhone 5 F	VL	various	11
MICHE I2 [9]	628	Apple iPhone 5 R	VL	various	12
MIR [35]	4500	Unknown Sensor	NIR	1968x1024	13
MMU2 [6]	995	Panas. BM-ET100US	NIR	320x238	14
MobBIO [32]	1640	Asus Eee Pad TE300T	VL	250x200	15
UBIRISv1 [29]	1876	Nikon E5700	VL	800x600	16
UBIRISv2 [30]	11102	Canon EOS 5D	VL	400x300	17
UPOL [10]	384	SONY DXC-950P	CF	768x576	18
UTIRIS [15]	793	ISG Lightwise LW	NIR	1000x776	19

Table 1. Attributes of iris datasets with number of images (#IMG), class ID (CID) and illumination (ILM). The illumination is either of the type near infrared (NIR), visible light (VL) or camera flash (CF).

3.2.3 Classification

A support vector machine (SVM) is used to classify the IFV encoded features. A linear kernel lead to the most promising results. The input data to the SVM (IFV encoded feature vectors) is normalised such that $K(x', x'') = 1$ which usually improves the performance. The SVM is trained using a standard non-linear SVM solver.

4. Experimental Setup

This section describes the examined datasets as well as the experimental setup.

4.1. Datasets

Table 1 summarises the most important attributes of the 19 publicly available datasets used in this work and Figure 3 shows one example image for each of the datasets. Each dataset was acquired with a distinct sensor model.

4.2. Experimental Methodology

Each dataset is randomly split into two distinct subsets, a training and a testing one. Since UPOL contains 384 images only, a 50:50 split of training and testing data results in a maximum of 192 training and 192 testing images. Datasets containing colour images are converted to greyscale. We tested different training set sizes $(1, 3, 6, 12, 24, 48, 96$ and $192)$ with a fixed test set size of 192 images for all datasets. A 5-fold cross validation is performed and the mean results of all 5 runs are the final results shown below.

All experiments are performed using different patch sizes ranging from 64×64 up to 512×512 pixels, which are cropped from the image centre. Due to the correlation based similarity measure all extracted patches must have the same size, thus the number of admissible sensors to discriminate for the PSI approach decreases with increasing patch size because of the varying image sizes among the data sets. The investigation of all 19 sensors for the PSI approach is only possible with patch sizes of 64×64 and 128×128. The ITC approach is able to handle different image sizes, hence all 19 sensors can be investigated with all patch sizes.

For the Image Texture Classification (ITC) approach the first step consists in extracting the features from the image patches using DenseSIFT, DMD and LBP. Afterwards, the features are reduced in dimensionality using a GMM and then Fisher Vector encoding is applied before they are put into a linear SVM for classification.

For the PRNU based Sensor Identification (PSI) approach the PRNU is extracted from the mentioned image patches. The extraction is performed using a variety of denoising filter and PRNU enhancement combinations, which are listed in Table 2. The interested reader is referred to the respective papers for further details on the PRNU extraction and enhancement techniques.

Name	Denoising filter	Noise residuals	Fingerprints
Li [19]	$Wavelet_{Lukas}$	Li Model 3	-
BM3D [7]	$BM3D$	-	-
FS [20]	$Wavelet_{Mihcak}$	FDR+Li	SEA

Table 2. Enhancement configurations applied to the different steps of the PRNU extraction process.

The generation of the PRNU fingerprints for the various sensors is done using the images from the "training" set. Then the NCC scores are computed for all "test" images with all generated PRNU fingerprints, where the predicted sensor (or class) is determined by means of the highest (rank one) correlation score.

Considering the score level fusion used in this work, we examined different normalisation (Minimum-Maximum, Tangens Hyperbolicus and Z-Score) and fusion schemes (Maximum, Average, Sum and Product). We tested different score combinations, from pairs of 2 scores to tuples of all 4 available scores (PSI, and the 3 ITC configurations). The Minimum-Maximum normalisation in combination with the Sum or Product fusion rule performed best across all combinations.

The following three experiments have been conducted to quantify the performance of the different techniques in discriminating between the various sensor.

Experiment 1 (EX1): Sensor Identification
The discriminability of the sensors of all iris data sets described in Table 1 using the 3 ITC (DenseSIFT, DMD, LBP) and 3 PSI (Li, BM3D, FS) configurations with 192 training and 192 test images is assessed. A patch size of 128 is used to be able to evaluate the performance for all sensors. Eventually, a score level fusion has been investigated.

Experiment 2 (EX2): Varying Patch/Training Set Sizes
Here the impact of the number of training images on the sensor identification performance of the ITC and PSI techniques is investigated. In contrast to the first experiment different training set sizes from 192 down to 1 and different patch sizes from 512 to 64 are examined. Again, a score level fusion has been investigated.

Experiment 3 (EX3): Intra-Model Sensor Identification
This experiment differs from the first two. The goal is to investigate whether the PSI and ITC techniques are able to distinguish different instances of the same sensor model. Since this is not possible with the biometric data described in Table 1, images from 6 different camera models (Casio EX-Z150, Kodak M1063, Nikon S710, Olympus MJU, Praktica DCZ 5.9 and Ricoh GX100) with 5 camera instances each have been selected from the Dresden database [14] to at least clarify this issue in general. The patch size for this experiment is 512. The training set size and test set size are set to 100 and 50, respectively, because of the low number of images available for some cameras. The discriminability of the instances has been evaluated separately for each camera model.

5. Experimental Results

In the following the results are presented and discussed. Based on the outcome of EX1 only the best performing ITC and PSI approaches have been considered for EX2 and EX3, which are: DSIFT, DMD, LBP and BM3D. The mean accuracy (mAcc) corresponds to the mean of the values of the confusion matrix diagonal. The average precision (AP) describes the area under the precision/recall curve calculated per class. The mAP is the mean over all AP values.

Experiment 1 The first results listed in Table 3 are devoted to EX1. It can be seen that DSIFT performs remarkably well in distinguishing the origin of images between the various iris datasets. Figure 4 (top) confirms that DSIFT is able to determine the origin of an iris image with a very high accuracy for all of the datasets. The different PSI configurations are inferior compared to the ITC approaches. On one hand, the patch size of 128 is relatively small for a PRNU approach. On the other hand, Figure 4 (bottom) reveals that especially the classes 2, 4, 5, 15, 16 and 17 cause problems. The numbers on the axes correspond to the class IDs in Table 1. The CASIA V3 (class ID 2) dataset is suspect to contain images from multiple sensors of the same model, as already reported in literature [34, 11]. The images from the MobBIO, UBIRISv1 and UBIRISv2 datasets (classes 15, 16 and 17) have been acquired with a high resolution camera. After thorough investigation we found out that the images contained in the datasets have been cropped from different parts of the original image which causes low correlation scores for images within the same dataset. To overcome this problem these images have to be pre-aligned e.g. by using a PRNU based approach [17] or by using the peak correlation energy (PCE) measure [13]. The best score level fusion combination BDDF, which denotes the fusion of BM3D-DSIFT-DMD, improves the identification performance to a small degree.

	DSIFT	DMD	LBP	BM3D	Li	FS	BDDF
mACC	98.78	88.51	91.96	67.82	65.92	60.20	99.48
mAP	99.51	91.23	95.05	67.93	65.26	40.72	99.86

Table 3. Mean accuracy (mACC) and mean average precision (mAP) for patch size 128 and training set size 192 for all iris datasets.

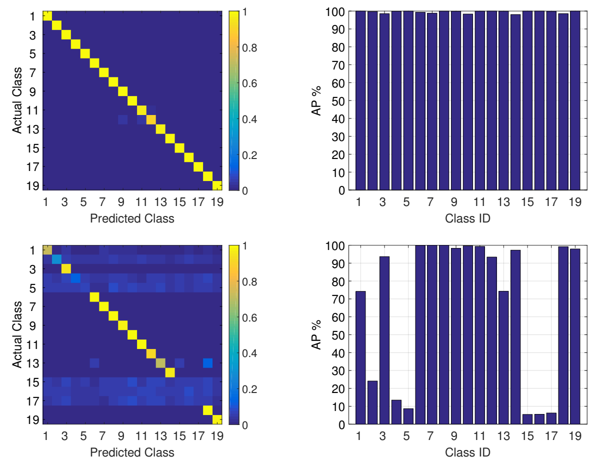

Figure 4. Confusion matrix and average precision plot for patch size 128 and training set size 192. Top: DSIFT, Bottom: BM3D.

Experiment 2 Table 4 and Figure 5 give an overview of the results for varying patch sizes and training set sizes for ITC, PSI and the fusion combination BDDF. To keep the results concise we only list some of the tested configurations. It is interesting to see that the performance of the ITC ap-

PS	TSS	mACC DSIFT	mACC DMD	mACC LBP	mACC BM3D	mACC BDDF	mAP DSIFT	mAP DMD	mAP LBP	mAP BM3D	mAP BDDF
512	192	99.92	86.09	97.96	90.27	99.96	99.98	87.17	99.12	90.23	99.99
512	24	98.90	83.07	87.50	88.89	99.18	99.49	84.61	90.16	89.14	99.59
512	3	93.16	73.59	0.00	79.63	92.69	95.19	75.56	0.00	81.08	94.86
256	192	99.64	90.70	96.67	75.03	99.87	99.92	91.80	98.22	75.52	99.97
256	24	97.96	87.90	80.04	70.70	98.30	98.93	88.10	81.97	70.75	99.16
256	3	89.29	74.58	0.00	55.38	88.31	91.85	75.62	0.00	55.30	91.29
128	192	98.78	88.51	91.96	67.82	99.48	99.52	91.23	95.05	67.93	99.68
128	24	94.78	83.76	67.75	57.48	95.49	96.48	84.36	68.31	57.00	97.13
128	3	80.26	67.09	0.00	34.23	78.79	84.13	68.03	0.00	32.37	83.67
64	192	94.95	86.86	84.07	50.93	97.69	97.13	87.59	87.77	48.21	99.01
64	24	85.57	76.28	55.05	35.28	88.32	89.13	77.27	53.31	30.34	92.03
64	3	62.91	53.17	0.00	18.68	65.75	67.78	54.36	0.00	14.83	71.18

Table 4. Results for different patch (PS) and training set sizes (TSS).

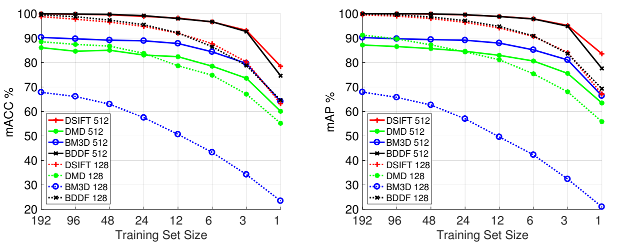

Figure 5. Results for selected patch sizes and different training set sizes.

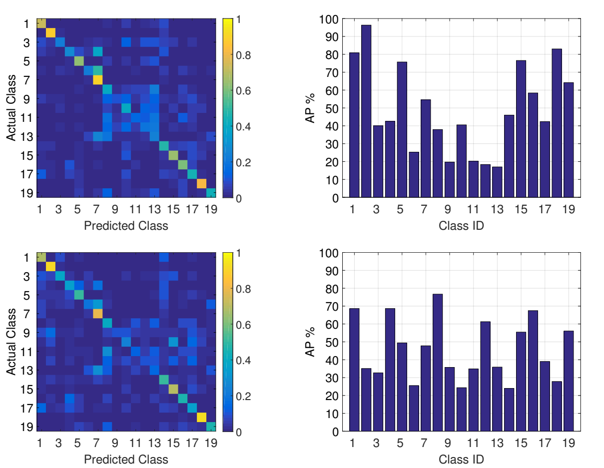

Figure 6. Confusion matrix and average precision plot for patch size 64 and training set size 1. Top: BDDF, Bottom: DSIFT.

proaches is insensitive to the training set size down to 24 images, whereas BM3D in combination with smaller patch sizes exhibits a constant performance drop towards smaller training set sizes. For larger patch sizes BM3D's performance interestingly remains almost stable down to 12 training images and its performance degrades less than the other approaches. Again fusion does not improve the overall performance, except in the case of a single training image.

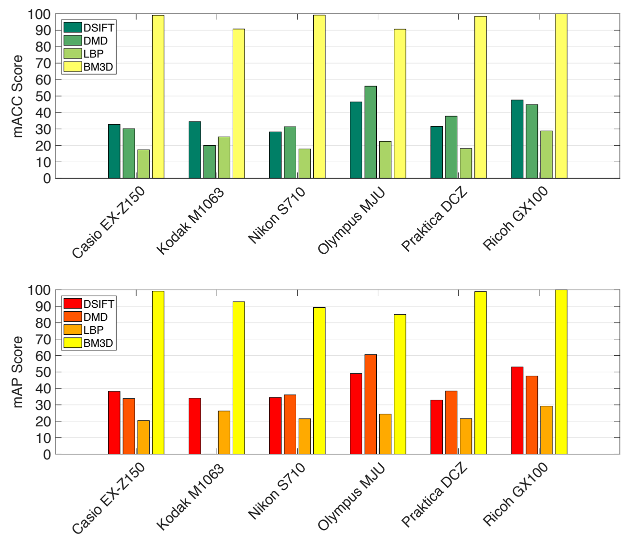

Figure 7. Results for the different camera models from the Dresden dataset with patch size 512 and training set size 100.

In Figure 6 we look at the most challenging case, patch size 64 and training set size 1, in more detail. As it can be seen in the confusion matrix and average precision plot for BDDF fusion the identification performance varies highly among the different classes resulting in an mAP of 49.45% and mACC of 46.28%. DSIFT achieves an mAP of 45.61% and mACC of 43.83% respectively. While the fusion gains accuracy for some classes (e.g. $1, 2, 15, 18$), it decreases the accuracy for other classes, leading to a slightly improved overall accuracy.

Experiment 3 This experiment reveals some interesting results regarding intra-model discrimination, which are presented in Figure 7. The BM3D approach reliably discriminates multiple instances of the same sensor model and exhibits mACC and mAP scores in the range of 82% to 100%, respectively. Despite the large patch and training set size, the ITC approaches face severe problems, with mACC and mAP scores between 0% and 60%. The ITC results strongly suggest that this approach is not useful to distinguish multiple instances of the same sensor model for arbitrary images.

5.1. Application Specific Discussion

As motivated in the introduction, identification of the image origin plays a major role for the security and performance of an iris recognition system. While it is sufficient to distinguish the origin at model level for performance enhancements, it is necessary to distinguish the origin at unit level to strengthen the security of the system.

It can be clearly seen that both, the ITC and PSI approach, are able to identify the source sensor model (i.e. iris dataset) of iris images in general. Eventually, our ITC approach outperformed the previous approach by El Naggar *et al*. [11]. However, our approach differs from the one by El Naggar *et al*., which uses unrolled iris textures for the identification of the datasets.

The PSI approach is mostly limited by the patch size and therefore faces limited application with sensors that output low-resolution images. Pre-alignment of the images or PCE as similarity measure is necessary for the PSI approach to work properly if arbitrary cropped and resized images are present. ITC works well in distinguishing the sensor model, provided that there are sufficient training images available (more than 12). It still works for small patch sizes and especially for the classes where the PSI approach is no longer able to provide a reasonable accuracy. Consequently, the ITC approach is well suited to provide the sensor model in the context of the selective processing scenario.

The results of EX3 exposed a weakness of the ITC approach, in distinguishing arbitrary natural scene images acquired with multiple instances of the same sensor model. Hence, the ITC approach might not be the preferred solution for the insertion attack detection scenario. Following Kerckhoff's principle, i.e. assuming that an attacker knows how the whole biometric system is designed, he could simply use the same sensor model as deployed in the system to acquire a malicious image, which could then successfully bypass an ITC based attack detection system. However, as pointed out by the EX3 results, the PSI approach is able to successfully discriminate different instances of the same sensor model. Therefore, the PSI approach is able to detect such a maliciously acquired and inserted image, but its performance depends on the patch size.

Obviously, a combination of both, the ITC and PSI approach, is beneficial to overcome the individual weaknesses and improve the detection of insertion attacks. We realised this combination in form of a score level fusion. The experimental results confirmed a performance improvement.

6. Conclusion

In this paper we investigated a passive approach to deduce sensor information solely from iris images. This information is useful in forensic scenarios, e.g. for for securing an iris recognition system against insertion attacks, as well as in non-forensic ones, e.g. to enable sensor model specific selective processing of the images. Our approach is based on two different techniques, a PRNU (PSI) and a texture classification one (ITC). In addition a score level fusion of the two different techniques is investigated to further improve the performance. Our experiments include tests using different numbers of training images as well as different image patch sizes.

The results confirm that our approach is well suited to identify the source sensor model of a given iris images in all test cases. It achieves almost 100% accuracy given that the training set size and patch size are sufficiently large. It still works reasonably well even for low resolution input images. The PSI approach is able to distinguish different sensors at unit level, but requires a certain patch size. By combining ITC and PSI through score level fusion a unit-level discrimination becomes possible for a broad range of sensor configurations.

Since no biometric dataset covering several units of the same sensor model is publicly available, we aim at establishing such a dataset. Our future work will then include extended tests to shed more light at the unit-level discrimination performance of our approach as well as investigation of an open set scenario.

Overall, by identifying the image origin at model and unit level, our approach forms the basis for the application of sensor specific processing of the iris images and can be of particular interest for securing iris recognition systems.

References

[1] S. S. Arora, M. Vatsa, R. Singh, and A. Jain. On iris camera interoperability. In *2012 IEEE Fifth International Conference on Biometrics: Theory, Applications and Systems (BTAS)*, pages 346–352, Sept 2012.

[2] S. Banerjee and A. Ross. From image to sensor: Comparative evaluation of multiple prnu estimation schemes for identifying sensors from nir iris images. In *Proceedings of 5th International Workshop on Biometrics and Forensics (IWBF'17)*, Coventry, UK, 2017.

[3] N. Bartlow, N. Kalka, B. Cukic, and A. Ross. Identifying sensors from fingerprint images. In *Computer Vision and Pattern Recognition Workshops, 2009. CVPR Workshops 2009. IEEE Computer Society Conference on*, pages 78–84, 2009.

[4] M. Chen, J. Fridrich, M. Goljan, and J. Lukas. Determining image origin and integrity using sensor noise. *IEEE Transactions on Information Security and Forensics*, 3(1):74–90, 2008.

[5] M. Cimpoi, S. Maji, I. Kokkinos, S. Mohamed, and A. Vedaldi. Describing textures in the wild. In *Proceedings of the IEEE Conference on Computer Vision and Pattern Recognition (CVPR'14)*, pages 3606–3613, 2014.

[6] Cteo. Mmu2 iris image database. *Available at: http://pesona.mmu.edu.my/ ccteo/*, 2008.

[7] K. Dabov, A. Foi, V. Katkovnik, and K. Egiazarian. Image denoising with block-matching and 3d filtering. In *Electronic Imaging 2006*, pages 606414–606414. International Society for Optics and Photonics, 2006.

[8] J. Daugman. How iris recognition works. *IEEE Transactions on Circiuts and Systems for Video Technology*, 14(1):21–30, 2004.

[9] M. De Marsico, M. Nappi, D. Riccio, and H. Wechsler. Mobile iris challenge evaluation (MICHE)-I, biometric iris dataset and protocols. *Pattern Recogn. Lett.*, 57(C):17–23, May 2015.

[10] M. Dobes and L. Machala. Upol iris image database, 2004. *Available at: http;//www.phoenix.inf.upol.cz/iris*, 2013.

[11] S. El-Naggar and A. Ross. Which dataset is this iris image from? In *Information Forensics and Security (WIFS), 2015 IEEE International Workshop on*, pages 1–6. IEEE, 2015.

[12] L. Fei-Fei and P. Perona. A bayesian hierarchical model for learning natural scene categories. In *Computer Vision and Pattern Recognition, 2005. CVPR 2005. IEEE Computer Society Conference on*, volume 2, pages 524–531 vol. 2. IEEE, 2005.

[13] J. Fridrich. Digital image forensic using sensor noise. *IEEE Signal Processing Magazine*, 26(2), 2009.

[14] T. Gloe and R. Böhme. The dresden image database for benchmarking digital image forensics. In *SAC 2010: Proceedings of the 2010 ACM Symposium on Applied Computing*, pages 1584–1590, 2010.

[15] M. Hosseini, B. Araabi, and H. Soltanian-Zadeh. Pigment melanin: Pattern for iris recognition. *Instrumentation and Measurement, IEEE Transactions on*, 59(4):792 –804, 2010.

[16] N. Kalka, N. Bartlow, B. Cukic, and A. Ross. A preliminary study on identifying sensors from iris images. In *The IEEE Conference on Computer Vision and Pattern Recognition (CVPR) Workshops*, 2015.

[17] C. Kauba and A. Uhl. Prnu-based image alignment for defective pixel detection. In *Proceedings of the IEEE Eighth International Conference on Biometrics: Theory, Applications, and Systems (BTAS2016)*, pages 1–6, Niagara Falls, Buffalo, New York, USA, 2016.

[18] A. Kumar and A. Passi. Comparison and combination of iris matchers for reliable personal authentication. *Pattern recognition*, 43(3):1016–1026, 2010.

[19] C.-T. Li. Source camera identification using enhanced sensor pattern noise. *IEEE Transactions on Information Forensics and Security*, 5(2):280–287, 2010.

[20] X. Lin and C.-T. Li. Enhancing sensor pattern noise via filtering distortion removal. *IEEE Signal Processing Letters*, 23(3):381–385, 2016.

[21] D. G. Lowe. Distinctive image features from scale-invariant keypoints. *Int. J. Comput. Vision*, 60(2):91–110, 2004.

[22] F. Marra, G. Poggi, C. Sansone, and L. Verdoliva. A deep learning approach for iris sensor model identification. *Pattern Recognition Letters*, pages 1–9, 2017. to appear.

[23] R. Mehta and K. Egiazarian. *Texture Classification Using Dense Micro-block Difference (DMD)*, pages 643–658. Lecture Notes in Computer Science. Springer-Verlag, Berlin, 2015.

[24] M. Mihcak, I. Kozintsev, and K. Ramchandran. Spatially adaptive statistical modeling of wavelet image coefficients and its application to denoising. In *Proceedings of the 1999 IEEE International Conference on Acoustics, Speech, and Signal Processing, ICASSP '99*, pages 3253–3256, Phoenix, AZ, USA, Mar. 2009. IEEE.

[25] N. L. of Pattern Recognition. Casia Iris V4 Database. `http://biometrics.idealtest.org/findTotalDbByMode.do?mode=Iris`.

[26] N. L. of Pattern Recognition. ICB Competition on Cross-sensor Iris Recognition (CSIR2015). `http://biometrics.idealtest.org/2015/csir2015.jsp`.

[27] T. Ojala, M. Pietikainen, and D. Harwood. Performance evaluation of texture measures with classification based on kullback discrimination of distributions. In *Proceedings of the 12th IAPR International Conference on Pattern Recognition*, volume 1, pages 582 –585 vol.1, 1994.

[28] P. J. Phillips, K. W. Bowyer, P. J. Flynn, X. Liu, and W. T. Scruggs. The iris challenge evaluation 2005. In *Biometrics: Theory, Applications and Systems, 2008. BTAS 2008. 2nd IEEE International Conference on*, pages 1–8. IEEE, 2008.

[29] H. Proenca and L. A. Alexandre. Toward Noncooperative Iris Recognition: A Classification Approach Using Multiple Signatures. *IEEE Transactions on Pattern Analysis and Machine Intelligence*, 29(4):607–612, April 2007.

[30] H. Proenca, S. Filipe, R. Santos, J. Oliveira, and L. Alexandre. The UBIRIS.v2: A database of visible wavelength images captured on-the-move and at-a-distance. *IEEE Trans. PAMI*, 32(8):1529–1535, August 2010.

[31] N. Ratha, J. Connell, and R. Bolle. Enhancing security and privacy in biometrics-based authentication systems. *IBM Systems Journal*, 40(3):614–634, 2001.

[32] A. F. Sequeira, J. C. Monteiro, A. Rebelo, and H. P. Oliveira. MobBIO: A multimodal database captured with a portable handheld device. In *2014 International Conference on Computer Vision Theory and Applications (VISAPP)*, volume 3, pages 133–139, Jan 2014.

[33] A. Tuama, F. Comby, and M. Chaumont. Camera model identification with the use of deep convolutional neural networks. In *2016 IEEE International Workshop on Information Forensics and Security (WIFS)*, pages 1–6, Dec 2016.

[34] A. Uhl and Y. Höller. Iris-sensor authentication using camera PRNU fingerprints. In *Proceedings of the 5th IAPR/IEEE International Conference on Biometrics (ICB'12)*, pages 1–8, New Delhi, India, 2012.

[35] M. Zhang, Q. Zhang, Z. Sun, S. Zhou, and N. U. Ahmed. The BTAS*Competition on Mobile Iris Recognition. In *2016 IEEE 8th International Conference on Biometrics Theory, Applications and Systems (BTAS)*, pages 1–7, Sept 2016.